An Open-System Quantum Simulator with Trapped Ions

Julio T. Barreiro*[,1], Markus Müller*[,2,3], Philipp Schindler[1], Daniel Nigg[1], Thomas Monz[1], Michael Chwalla[1,2], Markus Hennrich[1], Christian F. Roos[1,2], Peter Zoller[2,3] and Rainer Blatt[1,2]

[1] *Institut für Experimentalphysik, Universität Innsbruck, Technikerstr. 25, 6020 Innsbruck, Austria*

[2] *Institut für Quantenoptik und Quanteninformation, Österreichische Akademie der Wissenschaften, Technikerstr. 21A, 6020 Innsbruck, Austria*

[3] *Institut für Theoretische Physik, Universität Innsbruck, Technikerstr. 25, 6020 Innsbruck, Austria*

* *These authors contributed equally to this work.*

The control of quantum systems is of fundamental scientific interest and promises powerful applications and technologies. Impressive progress has been achieved in isolating the systems from the environment and coherently controlling their dynamics, as demonstrated by the creation and manipulation of entanglement in various physical systems. However, for open quantum systems, engineering the dynamics of many particles by a controlled coupling to an environment remains largely unexplored. Here we report the first realization of a toolbox for simulating an open quantum system with up to five qubits. Using a quantum computing architecture with trapped ions, we combine multi-qubit gates with optical pumping to implement coherent operations and dissipative processes. We illustrate this engineering by the dissipative preparation of entangled states, the simulation of coherent many-body spin interactions and the quantum non-demolition measurement of multi-qubit observables. By adding controlled dissipation to coherent operations, this work offers novel prospects for open-system quantum simulation and computation.

Every quantum system is inevitably coupled to its surrounding environment. Significant progress has been made in isolating systems from their enviroment and coherently controlling the dynamics of several qubits [1–4]. These achievements have enabled the realization of high-fidelity quantum gates, the implementation of small-scale quantum computing and communication devices as well as the measurement-based probabilistic preparation of entangled states, in atomic [5, 6], photonic [7] and solid-state setups [8–10]. In particular, successful demonstrations of quantum simulators [11, 12], which allow one to mimic and study the dynamics of complex quantum systems, have been reported [13].

In contrast, controlling the more general dynamics of open systems amounts to engineering both the Hamiltonian time evolution of the system as well as the coupling to the environment. Although open-system dynamics in a many-body or multi-qubit system are typically associated with decoherence [14–16], the ability to design dissipation can be a useful resource. For example, controlled dissipation allows the preparation of a desired entangled state from an arbitrary state [17–19] or an enhanced sensitivity for precision measurements [20]. In a broader context, by combining suitably chosen coherent and dissipative time steps, one can realize the most general non-unitary open-system evolution of a many-particle system. This engineering of the system-environment coupling generalizes the concept of Hamiltonian quantum simulation to open quantum systems. In addition, this engineering enables the dissipative preparation and manipulation of many-body states and quantum phases [21], and also quantum computation based on dissipation [22].

Here we provide the first experimental demonstration of a complete toolbox, through coherent and dissipative manipulations of a multi-qubit system, to control the dynamics of open systems. In a string of trapped ions, each ion encoding a qubit, we subdivide the qubits into "system" and "environment". The system-environment coupling is then engineered through the universal set of quantum operations available in ion-trap quantum computers [23, 24] and a dissipative mechanism based on optical pumping.

We first illustrate this engineering by dissipatively preparing a Bell state in a 2+1 ion system, such that an initially fully mixed state is pumped into a given Bell state. Similarly, with 4+1 ions, we also dissipatively prepare a 4-qubit GHZ-state, which can be regarded as a minimal instance of Kitaev's toric code [25]. Besides the dissipative elements, we show coherent n-body interactions by implementing the fundamental building block for 4-spin interactions. In addition, we demonstrate a read-out of n-particle observables in a non-destructive way with a quantum-nondemolition (QND) measurement of a 4-qubit stabilizer operator. Altogether, our work demonstrates all essential coherent and dissipative elements for controlling general open-system dynamics.

OPEN-SYSTEM QUANTUM DYNAMICS AND BELL-STATE "COOLING"

The dynamics of an open quantum system S coupled to an environment E can be described by the unitary transformation $\rho_{SE} \mapsto U\rho_{SE}U^\dagger$, with ρ_{SE} the joint density matrix of the composite system $\mathrm{S}+\mathrm{E}$. Thus, the reduced density operator of the system will evolve as

$\rho_S = \mathrm{Tr}_E U \rho_{SE} U^\dagger$. The time evolution of the system can also be described by a completely positive Kraus map

$$\rho_S \mapsto \mathcal{E}(\rho_S) = \sum_k E_k \rho_S E_k^\dagger \tag{1}$$

with E_k operation elements satisfying $\sum_k E_k^\dagger E_k = 1$ [26]. If the system is decoupled from the environment, the general map (1) reduces to $\rho_S \mapsto U_S \rho_S U_S^\dagger$, with U_S the unitary time evolution operator acting only on the system.

Control of both coherent and dissipative dynamics is then achieved by finding corresponding sequences of maps (1) specified by sets of operation elements $\{E_k\}$ and engineering these sequences in the laboratory. In particular, for the example of dissipative quantum state preparation, pumping to an entangled state $|\psi\rangle$ reduces to implementing appropriate sequences of dissipative maps. These maps are chosen to drive the system to the desired target state irrespective of its initial state. The resulting dynamics have then the pure state $|\psi\rangle$ as the unique attractor, $\rho_S \mapsto |\psi\rangle\langle\psi|$. In quantum optics and atomic physics, the techniques of optical pumping and laser cooling are successfully used for the dissipative preparation of quantum states, although on a *single-particle* level. The engineering of dissipative maps for the preparation of entangled states can be seen as a generalization of this concept of pumping and cooling in driven dissipative systems to a *many-particle* context. To be concrete, we focus on dissipative preparation of stabilizer states, which represent a large family of entangled states, including graph states and error-correcting codes [27].

We start by outlining the concept of Kraus map engineering for the simplest non-trivial example of "cooling" a system of two qubits into a Bell state. The Hilbert space of two qubits is spanned by the four Bell states defined as $|\Phi^\pm\rangle = \frac{1}{\sqrt{2}}(|00\rangle \pm |11\rangle)$ and $|\Psi^\pm\rangle = \frac{1}{\sqrt{2}}(|01\rangle \pm |10\rangle)$. Here, $|0\rangle$ and $|1\rangle$ denote the computational basis of each qubit, and we use the short-hand notation $|00\rangle = |0\rangle_1|0\rangle_2$, for example. These maximally entangled states are stabilizer states: the Bell state $|\Phi^+\rangle$, for instance, is said to be *stabilized* by the two stabilizer operators Z_1Z_2 and X_1X_2, where X and Z denote the usual Pauli matrices, as it is the only two-qubit state being an eigenstate of eigenvalue $+1$ of these two commuting observables, i.e. $Z_1Z_2|\Phi^+\rangle = |\Phi^+\rangle$ and $X_1X_2|\Phi^+\rangle = |\Phi^+\rangle$. In fact, each of the four Bell states is uniquely determined as an eigenstate with eigenvalues ± 1 with respect to Z_1Z_2 and X_1X_2. The key idea of cooling is that we can achieve dissipative dynamics which pump the system into a particular Bell state, for example $\rho_S \mapsto |\Psi^-\rangle\langle\Psi^-|$, by constructing two dissipative maps, under which the two qubits are irreversibly transfered from the $+1$ into the -1 eigenspaces of Z_1Z_2 and X_1X_2.

The dissipative maps are engineered with the aid of an ancilla "environment" qubit [28, 29] and a quantum circuit of coherent and dissipative operations. The form and decomposition of these maps into basic operations are discussed in Box 1. The cooling dynamics are determined by the probability of pumping from the $+1$ into the -1 stabilizer eigenspaces, which can be directly controlled by varying the parameters in the employed gate operations. For pumping with unit probability ($p = 1$), the two qubits reach the target Bell state — regardless of their initial state — after only one cooling cycle, i.e., by a single application of each of the two maps. In contrast, when the pumping probability is small ($p \ll 1$), the process can be regarded as the infinitesimal limit of the general map (1). In this case, the system dynamics under a repeated application of the cooling cycle are described by a master equation [30]

$$\dot{\rho}_S = -i[H_S, \rho_S] + \sum_k \left(c_k \rho_S c_k^\dagger - \frac{1}{2} c_k^\dagger c_k \rho_S - \rho_S \frac{1}{2} c_k^\dagger c_k \right). \tag{2}$$

Here, H_S is a system Hamiltonian, and c_k are Lindblad operators reflecting the system-environment coupling. For the purely dissipative maps discussed here, $H_S = 0$. Quantum jumps from the $+1$ into the -1 eigenspace of Z_1Z_2 and X_1X_2 are mediated by a set of *two-qubit* Lindblad operators (see box 1 for details); here the system reaches the target Bell state asymptotically after many cooling cycles.

EXPERIMENTAL BELL-STATE COOLING

The dissipative preparation of n-particle entangled states is realized in a system of $n+1$ $^{40}Ca^+$ ions confined to a string by a linear Paul trap and cooled to the ground state of the axial centre-of-mass mode [31]. For each ion, the internal electronic Zeeman levels $D_{5/2}(m = -1/2)$ and $S_{1/2}(m = -1/2)$ encode the logical states $|0\rangle$ and $|1\rangle$ of a qubit. For coherent operations, a laser at a wavelength of 729 nm excites the quadrupole transition connecting the qubit states ($S_{1/2} \leftrightarrow D_{5/2}$). A broad beam of this laser couples to all ions (see Fig. 1a) and realizes the collective single-qubit gate $U_X(\theta) = \exp(-i\frac{\theta}{2}\sum_i X_i)$ as well as a Mølmer-Sørensen [32] (MS) entangling operation $U_{X^2}(\theta) = \exp(-i\frac{\theta}{4}(\sum_i X_i)^2)$ when using a bichromatic light field [33]. Shifting the optical phase of the drive field by $\pi/2$ exchanges X_i by Y_i in these operations. As a figure of merit of our entangling operation, we can prepare 3 (5) qubits in a GHZ state with 98% (95%) fidelity [34]. These collective operations form a universal set of gates when used in conjuction with single-qubit rotations $U_{Z_i}(\theta) = \exp(-i\frac{\theta}{2}Z_i)$, which are realized by an off-resonant laser beam that can be adjusted to focus on any ion.

For engineering dissipation, the key element of the mapping steps, shown as (i) and (iii) in Box 1, is a single MS operation. The two-qubit gate, step (ii), is real-

Box 1: Engineering dissipative open-system dynamics

Dissipative dynamics which cool two qubits from an arbitrary initial state into the Bell state $|\Psi^-\rangle$ are realized by two maps that generate pumping from the +1 into the -1 eigenspaces of the stabilizer operators Z_1Z_2 and X_1X_2:

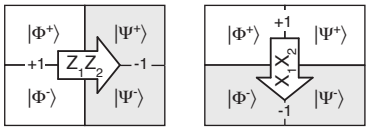

For Z_1Z_2, the dissipative map pumping into the -1 eigenspace is $\rho_S \mapsto \mathcal{E}(\rho_S) = E_1\rho_S E_1^\dagger + E_2\rho_S E_2^\dagger$ with

$$E_1 = \sqrt{p}\, X_2 \frac{1}{2}\left(1 + Z_1Z_2\right),$$
$$E_2 = \frac{1}{2}\left(1 - Z_1Z_2\right) + \sqrt{1-p}\,\frac{1}{2}\left(1 + Z_1Z_2\right).$$

The map's action as a uni-directional pumping process can be seen as follows. Since the operation element E_1 contains the projector $\frac{1}{2}(1+Z_1Z_2)$ onto the +1 eigenspace of Z_1Z_2, the spin flip X_2 can then convert +1 into -1 eigenstates of Z_1Z_2, e.g., $|\Phi^+\rangle \mapsto |\Psi^+\rangle$. In contrast, the -1 eigenspace of Z_1Z_2 is left invariant. In the limit $p \ll 1$, the repeated application of this map reduces the process to a master equation with Lindblad operator $c = \frac{1}{2}X_2(1 - Z_1Z_2)$.

We implement the two dissipative maps by quantum circuits of three unitary operations (i)-(iii) and a dissipative step (iv). Both maps act on the two system qubits S and an ancilla which plays the role of the environment E:

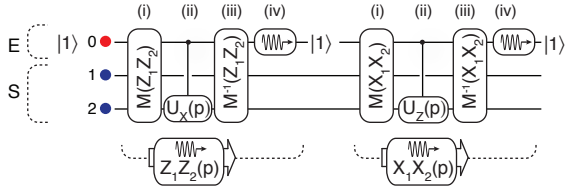

Cooling Z_1Z_2 proceeds as follows:

(i) Information about whether the system is in the +1 or -1 eigenspace of Z_1Z_2 is mapped by $M(Z_1Z_2)$ onto the logical states $|0\rangle$ and $|1\rangle$ of the ancilla (initially in $|1\rangle$).

(ii) A controlled gate $C(p)$ converts +1 into -1 eigenstates by flipping the state of the second qubit with probability p, where

$$C(p) = |0\rangle\langle 0|_0 \otimes U_{X_2}(p) + |1\rangle\langle 1|_0 \otimes \mathbb{1},$$

with $U_{X_2}(p) = \exp(i\alpha X_2)$ and $p = \sin^2\alpha$.

(iii) The initial mapping is inverted by $M^{-1}(Z_1Z_2)$. At this stage, in general, the ancilla and system qubits are entangled.

(iv) The ancilla is dissipatively reset to $|1\rangle$, which carries away entropy to "cool" the two system qubits.

The second map for cooling into the -1 eigenspace of X_1X_2 is obtained from interchanging the roles of X and Z above.

The engineering of dissipative maps can be readily generalized to systems of more qubits. As an example, dissipative preparation of n-qubit stabilizer states can be realized by a sequence of n dissipative maps (e.g. for Z_1Z_2 and $X_1X_2X_3X_4$ pumping), which are implemented in analogy to the quantum circuits for Bell state cooling discussed above:

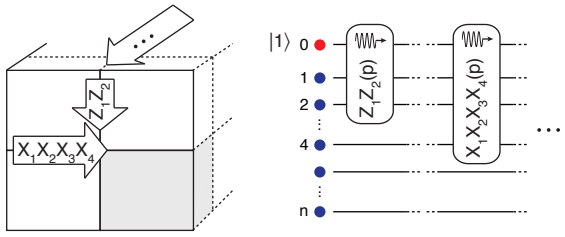

ized by a combination of collective and single-qubit operations. The dissipative mechanism, step (iv), is here carried out on the ancilla qubit by a reinitialization into $|1\rangle$, as shown in Fig. 1b. Another dissipative process [35] can be used to prepare the system qubits in a completely mixed state by the transfer $|0\rangle \rightarrow (|0\rangle + |S'\rangle)/\sqrt{2}$ followed by optical pumping of $|S'\rangle$ into $|1\rangle$, where $|S'\rangle$ is the electronic level $S_{1/2}(m = 1/2)$.

Qubit read-out is accomplished by fluorescence detection on the $S_{1/2} \leftrightarrow P_{1/2}$ transition. The ancilla qubit can be measured without affecting the system qubits by applying hiding pulses that shelve the system qubits in the $D_{5/2}$ state manifold during fluoresence detection [36].

We use these tools to implement up to three Bell-state cooling cycles on a string of 2+1 ions. Starting with the two system qubits in a completely mixed state, we cool towards the Bell state $|\Psi^-\rangle$. Each cooling cycle is accomplished with a sequence of 8 entangling operations, 4 collective unitaries and 6 single-qubit operations; see the Supplementary Information. The cooling dynamics are probed by quantum state tomography of the system qubits after every half cycle. The reconstructed states are then used to map the evolution of the Bell-state populations.

In a first experiment, we set the pumping probability at $p = 1$ to observe deterministic cooling, and we obtain the Bell-state populations shown in Fig. 2a. As expected, the system reaches the target state after the first cooling cycle. Regardless of experimental imperfections, the target state population is preserved under the repeated application of further cooling cycles and reaches up to 91(1)% after 1.5 cycles (ideally 100%). In a second experiment towards the simulation of master-equation dynamics, the probability is set at $p = 0.5$ to probe probabilistic cooling dynamics. The target state is then approached asymptotically (Fig. 2b). After cooling the system for 3 cycles with $p = 0.5$, up to 73(1)% of the initially mixed population cools into the target state (ideally 88%). In order to completely characterize the Bell-state cooling process, we also perform a quantum process tomography [26]. As an example, the reconstructed process matrix for $p = 1$ after 1.5 cycles (Fig. 2c) has a Jamiolkowski process fi-

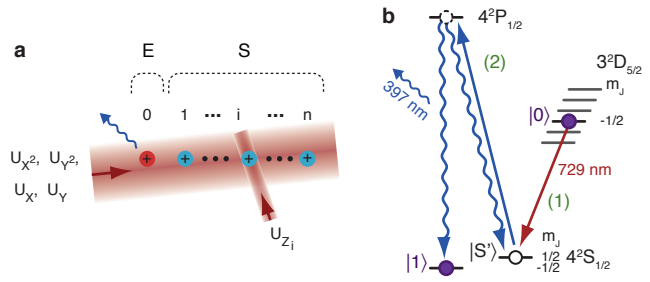

FIG. 1. **Experimental tools for the simulation of open quantum systems with ions. a,** The coherent component is realized by collective $(U_X, U_Y, U_{X^2}, U_{Y^2})$ and single-qubit operations (U_{Z_i}) on a string of $^{40}Ca^+$ ions which consists of the environment qubit (ion 0) and the system qubits (ions 1 through n). **b,** The dissipative mechanism on the ancilla qubit is realized in the two steps shown on the Zeeman-split $^{40}Ca^+$ levels by (1) a coherent transfer of the population from $|0\rangle$ to $|S'\rangle$ and (2) an optical pumping to $|1\rangle$ after a transfer to the $4^2P_{1/2}$ state by a circularly-polarised laser at 397 nm.

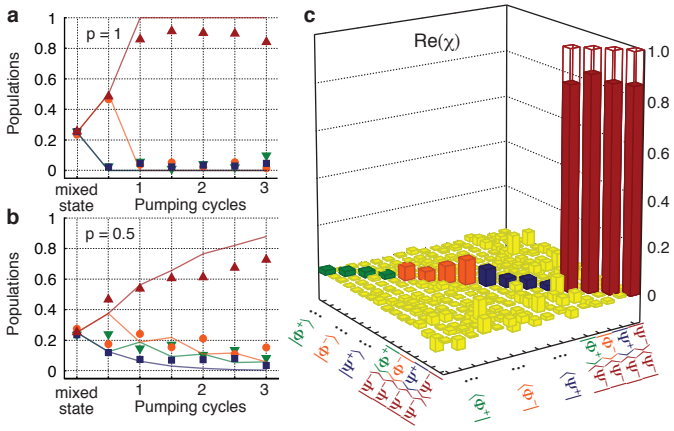

FIG. 2. **Experimental signatures of Bell-state cooling.** Evolution of the Bell-state populations $|\Phi^+\rangle$ (down triangles), $|\Phi^-\rangle$ (circles), $|\Psi^+\rangle$ (squares) and $|\Psi^-\rangle$ (up triangles) of an initially mixed state under a cooling process with probability **a,** $p = 1$ or deterministic and **b,** $p = 0.5$. Error bars, not shown, are smaller than 2% (1σ). **c,** Reconstructed process matrix χ (real part), displayed in the Bell-state basis, describing the deterministic cooling of the two ions after one and a half cycles. The ideal process mapping any input state into the state $|\Psi^-\rangle$ has as non-zero elements only the four transparent bars shown. The imaginary elements of χ, ideally all zero, have an average magnitude of 0.004 and a maximum of 0.03. The uncertainties in the elements of process matrix are smaller than 0.01 (1σ).

delity [37] of 87.0(7)% with the ideal dissipative process $\rho_S \mapsto |\Psi^-\rangle\langle\Psi^-|$ which maps an arbitrary state of the system into the Bell state $|\Psi^-\rangle$.

FOUR-QUBIT STABILIZER PUMPING

The engineering of the system-environment coupling, as demonstrated by Bell-state cooling above, can be readily extended to larger n-qubit open quantum systems. We illustrate such an engineering experimentally with the dissipative preparation of a four-qubit Greenberger-Horne-Zeilinger (GHZ) state $(|0000\rangle + |1111\rangle)/\sqrt{2}$. This state is uniquely characterized as the simultaneous eigenstate of the four stabilizers Z_1Z_2, Z_2Z_3, Z_3Z_4 and $X_1X_2X_3X_4$, all with eigenvalue +1 (see Fig. 3a). Therefore, cooling dynamics into the GHZ state are realized by four consecutive dissipative steps, each pumping the system into the +1 eigenspaces of the four stabilizers. In a system of 4+1 ions, we implement such cooling dynamics in analogy with the Bell-state cooling sequence. Here, however, the circuit decomposition of one cooling cycle involves 16 five-ion entangling operations, 20 collective unitaries and 34 single-qubit operations; further details in the Supplementary Information.

In order to observe this deterministic cooling process into the GHZ state, we begin by preparing the system ions in a completely mixed state. The evolution of the state of the system after each pumping step is characterized by quantum state tomography. The reconstructed density matrices shown in Fig. 3b for the initial and subsequent states arising in each step have a fidelity, or state overlap [38], with the expected states of {79(2),89(1),79.7(7),70.0(7),55.8(4)}%; see Supplementary Information for further details. Since the final state has a fidelity with the target GHZ state greater than 50%, the initially mixed state is cooled into a genuinely four-particle entangled state [39]. The pumping dynamics is clearly reflected by the measured expectation values of the stabilizers Z_iZ_j $(ij = 12, 23, 34, 14)$ and $X_1X_2X_3X_4$ at each step, as shown in Fig. 3c.

Although the simulation of a master equation requires small pumping probabilities, as an exploratory study, we implement up to five consecutive $X_1X_2X_3X_4$-stabilizer pumping steps with two probabilities $p = 1$ and 0.5, for the initial state $|1111\rangle$. The measured expectation values of all relevant stabilizers for pumping with $p = 1$ are shown in Fig. 3d. After the first step, the stabilizer $X_1X_2X_3X_4$ reaches an expectation value of -0.68(1); after the second step and up to the fifth step, it is preserved at -0.72(1) regardless of experimental imperfections.

For $X_1X_2X_3X_4$-stabilizer pumping with $p = 0.5$, the four-qubit expectation value increases at each step and asymptotically approaches -0.54(1) (ideally -1, fit shown in Fig. 3d). A state tomography after each pumping step yields fidelities with the expected GHZ-state of {53(1), 50(1), 49(1), 44(1), 41(1)}%. From the reconstructed density matrices we determine that the states generated after one to three cycles are genuinely multi-partite entangled [40].

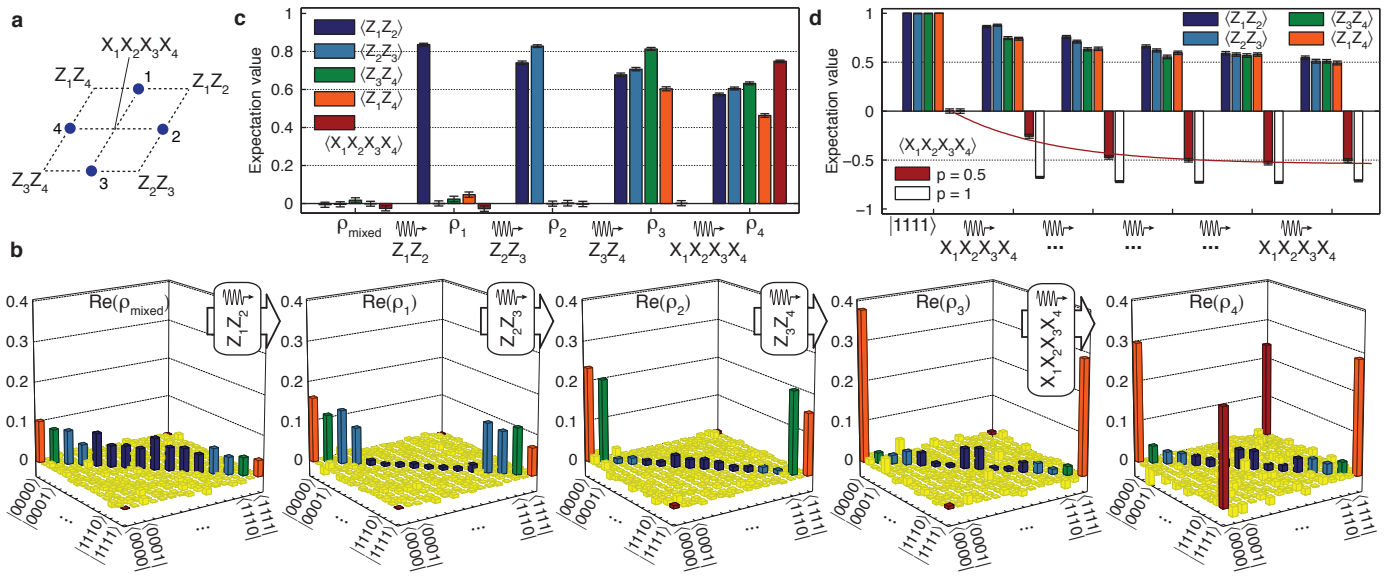

FIG. 3. **Experimental signatures of four-qubit stabilizer pumping. a,** Schematic of the four system qubits to be cooled into the GHZ state $(|0000\rangle + |1111\rangle)/\sqrt{2}$, which is uniquely characterized as the simultaneous eigenstate with eigenvalue $+1$ of the shown stabilizers. **b,** Reconstructed density matrices (real part) of the initial mixed state ρ_{mixed} and subsequent states $\rho_{1,2,3,4}$ after sequentially pumping the stabilizers Z_1Z_2, Z_2Z_3, Z_3Z_4 and $X_1X_2X_3X_4$. Populations in the initial mixed state with qubits i and j antiparallel, or in the -1 eigenspace of the Z_iZ_j stabilizer, disappear after pumping this stabilizer into the $+1$ eigenspace. For example, populations in dark blue dissappear after Z_1Z_2-stabilizer pumping. A final pumping of the stabilizer $X_1X_2X_3X_4$ builds up the coherence between $|0000\rangle$ and $|1111\rangle$, shown as red bars in the density matrix of ρ_4. **c,** Measured expectation values of the relevant stabilizers; ideally, non-zero expectation values have a value of $+1$. **d,** Evolution of the measured expectation values of the relevant stabilizers for repetitively pumping an initial state $|1111\rangle$ with probability $p = 0.5$ into the -1 eigenspace of the stabilizer $X_1X_2X_3X_4$. The incremental cooling is evident by the red line fitted to the pumped stabilizer expectation value. The evolution of the expectation value $\langle X_1X_2X_3X_4\rangle$ for deterministic cooling ($p = 1$) is also shown. The observed decay of $\langle Z_iZ_j\rangle$ is due to imperfections and detrimental to the pumping process (see Supplementary Information). Error bars in **c** and **d**, $\pm 1\sigma$.

COHERENT FOUR-PARTICLE INTERACTIONS

The coupling of the system to an ancilla particle, as used above for the engineering of dissipative dynamics, can also be harnessed to mediate effective coherent n-body interactions between the system qubits [26, 29]. The demonstration of a toolbox for open-system quantum simulation is thus complemented by adding unitary maps $\rho_S \mapsto U_S \rho_S U_S^\dagger$ to the dissipative elements described above. Here, $U_S = \exp(-i\tau H_S)$ is the unitary time evolution operator for a time step τ, which is generated by a system Hamiltonian H_S. In contrast to the recent achievements [41, 42] of small-scale analog quantum simulators based on trapped ions, where two-body spin Hamiltonians have been engineered directly [43], here we pursue a gate-based implementation following the concept of Lloyd's digital quantum simulator [12], where the time evolution is decomposed into a sequence of coherent (and dissipative) steps.

In particular, the available gate operations enable an *experimentally efficient* simulation of n-body spin interactions [44], which we illustrate by implementing time dynamics of a four-body Hamiltonian $H_S = gX_1X_2X_3X_4$. This example is motivated by the efforts to experimentally realize Kitaev's toric code Hamiltonian [25], which is a sum of commuting four-qubit stabilizer operators representing four-body spin interactions. This paradigmatic model belongs to a whole class of spin systems, which have been discussed in the context of topological quantum computing [45] and quantum phases exhibiting topological order [46].

The elementary unitary operation U_S can be decomposed into a compact sequence of three coherent operations, as explained in Fig. 4a. In an experiment carried out with 4+1 ions, we apply U_S for different values of τ to the system ions initially prepared in $|1111\rangle$. We observed coherent oscillations in the subspace spanned by $|0000\rangle$ and $|1111\rangle$, as shown in Fig. 4b. We characterize our implementation of U_S by comparing the expected and measured states, determined by quantum state tomography, for each value of τ. The fidelity between the expected and measured states is on average 85(2)%.

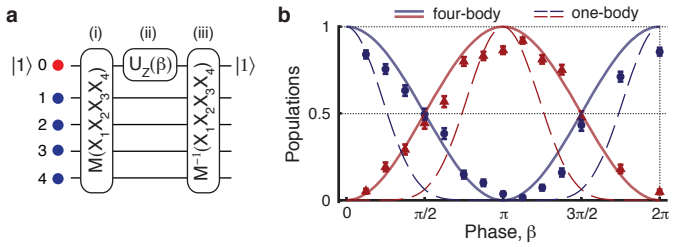

FIG. 4. **Coherent simulation of 4-body spin interactions. a,** The elementary building block for the simulation of coherent evolution $U_S = \exp(-i\tau H_S)$ corresponding to the four-body Hamiltonian $H_S = gX_1X_2X_3X_4$ is implemented by a circuit of three operations: (i) First, a 5-qubit operation $M(X_1X_2X_3X_4)$, here realized by a single entangling 5-ion MS gate $U_{S^2_x}(\pi/2)$, coherently maps the information, whether the four system spins are in the +1(-1) eigenspace of $X_1X_2X_3X_4$ onto the internal states $|0\rangle$ and $|1\rangle$ of the ancilla qubit. (ii) Due to this mapping, all +1 (-1) eigenstates of $X_1X_2X_3X_4$ acquire a phase $\beta/2$ $(-\beta/2)$ by the single-qubit rotation $U_Z(\beta)$ on the ancilla ion. (iii) After the mapping is inverted, the ancilla qubit returns to its initial state $|1\rangle$ and decouples from the four system qubits, which in turn have evolved according to U_S. The simulation time step τ is related to the phase by $\beta = 2g\tau$. **b,** Experimentally measured populations in state $|0000\rangle$ (up triangles) and $|1111\rangle$ (circles) as a function of β for a single application of U_S to the initial state $|1111\rangle$ of the four system qubits (error bars, $\pm 1\sigma$). The solid lines show the ideal behavior. For comparison, the dashes lines indicate these populations for simultaneous single-qubit (one-body) oscillations, each driven by the rotation $\exp(-i\frac{\beta}{2}X_i)$.

QND MEASUREMENT OF FOUR-QUBIT STABILIZER OPERATORS

Our toolbox for quantum simulation of open systems is extended by the possibility of reading out n-body observables in a nondestructive way, which we illustrate here for a 4-qubit stabilizer operator $X_1X_2X_3X_4$. As above, we first coherently map the information about whether the system spins are in the +1(-1) eigenspace of the stabilizer operator onto the logical states $|0\rangle$ and $|1\rangle$ of the ancilla qubit. In contrast to the engineering of coherent and dissipative maps above, where this step was followed by single-and two-qubit gate operations, here we proceed instead by measuring the ancilla qubit.

Thus, depending on the measurement outcome for the ancilla, the system qubits are projected onto the corresponding eigenspace of the stabilizer: $\rho_S \mapsto P_+\rho_S P_+/N_+$ $(P_-\rho_S P_-/N_-)$ for finding the ancilla in $|0\rangle$ $(|1\rangle)$ with the normalization factor $N_\pm = \mathrm{Tr}(P_\pm\rho_S P_\pm)$. Here, $P_\pm = \frac{1}{2}(1 \pm X_1X_2X_3X_4)$ denote the projectors onto the ± 1 eigenspaces of the stabilizer operator. Note that our measurement is QND in the sense that (superposition) states within one of the two eigenspaces are not affected by the measurement.

In the experiment with 4+1 ions, we prepare different four-qubit system input states (tomographically characterize in additional experiments), carry out the QND measurement and tomographically determine the resulting system output states.

To characterize how well the measurement device prepares a definite state, we use as input $|1111\rangle$, which is a non-eigenstate of the stabilizer. In this case, when the ancilla qubit is found in $|0\rangle$ or $|1\rangle$ the system qubits are prepared in the state $(|0000\rangle \pm |1111\rangle)/\sqrt{2}$ by the QND measurement. Experimentally we observe this behaviour with a quantum state preparation (QSP) fidelity [47] of $F_{\mathrm{QSP}} = 73(1)\%$. On the other hand, for a stabilizer eigenstate, the QND measurement preserves the stabilizer expectation value. Experimentally, for the input state $(|0011\rangle - |1100\rangle)/\sqrt{2}$, we observe a QND fidelity [47] of $F_{\mathrm{QND}} = 96.9(6)\%$. For more details see the Supplementary Information.

Our measurement of n-body observables is an essential ingredient in quantum error correction and quantum computing protocols. In contrast to the *open-loop* experiments presented here [28], this ability also enables an alternative approach for system-environment engineering: The outcome from measurements of the environment can be classically processed and used for feedback operations on the system. This procedure paves the way to *closed-loop* simulation scenarios in open quantum systems.

OUTLOOK

Our experimental demonstration of a toolbox of elementary building blocks in a system of trapped ions should be seen as a first, and conceptual step towards the realization of an open quantum system simulator, with dynamics governed by the interplay of coherent and dissipative evolution. Such a quantum device has applications in various fields [13] including condensed-matter physics and quantum chemistry, and possibly in modelling quantum effects in biology [48]. In addition to quantum simulation, it enables alternative approaches to quantum computing [22].

Although the present experiments were performed with a linear ion-trap quantum computer architecture, the ongoing development of two-dimensional trap arrays [49] promises scalable implementations of Kitaev's toric code [25] and related spin models, as discussed in the context of topological quantum computing. Following our original proposal [50], these ideas can be realized with neutral atoms in optical lattices and can be easily adapted to other physical platforms ranging from optical, atomic and molecular systems to solid-state devices.

ACKNOWLEDGMENTS

We would like to thank K. Hammerer, I. Chuang, and O. Gühne for discussions and T. Northup for critically

reading the manuscript. We gratefully acknowledge support by the Austrian Science Fund (FOQUS), the European Commission (AQUTE), the Institut für Quanteninformation GmbH, and a Marie Curie International Incoming Fellowship within the 7th European Community Framework Programme.

AUTHOR CONTRIBUTIONS

M.M. and J.T.B. developed the research, based on theoretical ideas proposed originally by P.Z.; J.T.B., P.S. and D.N. carried out the experiment; J.T.B., P.S. and T.M. analysed the data; P.S., J.T.B., D.N., T.M., M.C., M.H. and R.B. contributed to the experimental setup; M.M., J.T.B. and P.Z. wrote the manuscript, with revisions provided by C.F.R.; all authors contributed to the discussion of the results and manuscript.

[1] Ladd, T. D., Jelezko, F., Laflamme, R., Nakamura, Y., Monroe, C. *et al.* Quantum computers. *Nature* **464**, 45–53 (2010)

[2] Kimble, H. J. The quantum internet. *Nature* **453**, 1023–1030 (2008)

[3] Schoelkopf, R. J. & Girvin, S. M. Wiring up quantum systems. *Nature* **451**, 664–669 (2008)

[4] Neeley, M., Bialczak, R. C., Lenander, M., Lucero, E., Mariantoni, M. *et al.* Generation of three-qubit entangled states using superconducting phase qubits. *Nature* **467**, 570–573 (2010)

[5] Saffman, M., Walker, T. G. & Mølmer, K. Quantum information with Rydberg atoms. *Rev. Mod. Phys.* **82**, 2313–2363 (2010)

[6] Bloch, I., Dalibard, J. & Zwerger, W. Many-body physics with ultracold gases. *Rev. Mod. Phys.* **80**, 885–964 (2008)

[7] O'Brien, J. L. Optical quantum computing. *Science* **318**, 1567–1570 (2007)

[8] Clarke, J. & Wilhelm, F. K. Superconducting quantum bits. *Nature* **453**, 1031–1042 (2008)

[9] Hanson, R., Kouwenhoven, L. P., Petta, J. R., Tarucha, S. & Vandersypen, L. M. K. Spins in few-electron quantum dots. *Rev. Mod. Phys.* **79**, 1217–1265 (2007)

[10] Wrachtrup, J. & Jelezko, F. Processing quantum information in diamond. *J. Phys.: Condens. Matter* **18**, S807–S824 (2006)

[11] Feynman, R. Simulating physics with computers. *Int. J. Theor. Phys.* **21**, 467–488 (1982)

[12] Lloyd, S. Universal quantum simulators. *Science* **273**, 1073–1078 (1996)

[13] Buluta, I. & Nori, F. Quantum simulators. *Science* **326**, 108–111 (2009)

[14] Myatt, C. J. *et al.* Decoherence of quantum superpositions through coupling to engineered reservoirs. *Nature* **403**, 269–273 (2000)

[15] Deleglise, S., Dotsenko, I., Sayrin, C., Bernu, J., Brune, M. *et al.* Reconstruction of non-classical cavity field states with snapshots of their decoherence. *Nature* **455**, 510–514 (2008)

[16] Barreiro, J. T., Schindler, P., Gühne, O., Monz, T., Chwalla, M. *et al.* Experimental multiparticle entanglement dynamics induced by decoherence. *Nature Phys.* (2010). Advance Online Publication, doi:10.1038/nphys1781

[17] Krauter, H., Muschik, C. A., Jensen, K., Wasilewski, W., Petersen, J. M. *et al.* Entanglement generated by dissipation. *arXiv:1006.4344* (2010)

[18] Diehl, S. *et al.* Quantum states and phases in driven open quantum systems with cold atoms. *Nature Phys.* **4**, 878–883 (2008)

[19] Cho, J., Bose, S. & Kim, M. S. Optical pumping into many-body entanglement. *arXiv:1008.4088* (2010)

[20] Goldstein, G., Cappellaro, P., Maze, J. R., Hodges, J. S., Jiang, L. *et al.* Environment-assisted precision measurement. *arXiv:1001.0089* (2010)

[21] Diehl, S., Yi, W., Daley, A. & Zoller, P. Driven dissipative d-wave pairing of atomic fermions. *arXiv:1007.3420* (2010)

[22] Verstraete, F., Wolf, M. M. & Cirac, J. I. Quantum computation and quantum-state engineering driven by dissipation. *Nature Phys.* **5**, 633–636 (2009)

[23] Häffner, H., Roos, C. F. & Blatt, R. Quantum computing with trapped ions. *Phys. Rep.* **469**, 155–203 (2008)

[24] Home, J. P., Hanneke, D., Jost, J. D., Amini, J. M., Leibfried, D. *et al.* Complete methods set for scalable ion trap quantum information processing. *Science* **325**, 1227–1230 (2009)

[25] Kitaev, A. Y. Fault-tolerant quantum computation by anyons. *Ann. Phys.* **303**, 2 – 30 (2003)

[26] Nielsen, M. A. & Chuang, I. L. *Quantum Computation and Quantum Information*. Cambridge University Press (2000)

[27] Steane, A. M. Efficient fault-tolerant quantum computing. *Nature* **399**, 124–126 (1999)

[28] Lloyd, S. & Viola, L. Engineering quantum dynamics. *Phys. Rev. A* **65**, 010101 (2001)

[29] Dür, W., Bremner, M. J. & Briegel, H. J. Quantum simulation of interacting high-dimensional systems: The influence of noise. *Phys. Rev. A* **78**, 052325 (2008)

[30] Wiseman, H. M. & Milburn, G. J. *Quantum Measurement and Control*. Cambridge University Press (2009)

[31] Schmidt-Kaler, F. *et al.* How to realize a universal quantum gate with trapped ions. *App. Phys. B* **77**, 789–796 (2003)

[32] Mølmer, K. & Sørensen, A. Multiparticle entanglement of hot trapped ions. *Phys. Rev. Lett.* **82**, 1835–1838 (1999)

[33] Roos, C. F. Ion trap quantum gates with amplitude-modulated laser beams. *New J. Phys.* **10**, 013002 (2008)

[34] Monz, T. *et al.* Coherence of large-scale entanglement. *arXiv:1009.6126* (2010)

[35] Schindler, P. *et al.* Experimental repetitive quantum error correction. *In preparation* (2010)

[36] Roos, C. F. *et al.* Control and measurement of three-qubit entangled states. *Science* **304**, 1478–1480 (2004)

[37] Gilchrist, A., Langford, N. K. & Nielsen, M. A. Distance measures to compare real and ideal quantum processes. *Phys. Rev. A* **71**, 062310 (2005)

[38] Jozsa, R. Fidelity for mixed quantum states. *J. Mod. Opt.* **41**, 2315–2353 (1994)

[39] Sackett, C. A. *et al.* Experimental entanglement of four particles. *Nature* **404**, 256–259 (2000)

[40] Gühne, O. & Seevinck, M. Separability criteria for genuine multiparticle entanglement. *New J. Phys.* **12**,

053002 (2010)

[41] Friedenauer, A., Schmitz, H., Glueckert, J., Porras, D. & Schaetz, T. Simulating a quantum magnet with trapped ions. *Nature Phys.* **4**, 757–761 (2008)

[42] Kim, K., Chang, M.-S., Korenblit, S., Islam, R., Edwards, E. E. *et al.* Quantum simulation of frustrated ising spins with trapped ions. *Nature* **465**, 590–593 (2010)

[43] Porras, D. & Cirac, J. I. Effective quantum spin systems with trapped ions. *Phys. Rev. Lett.* **92**, 207901 (2004)

[44] Müller, M., Hammerer, K., Zhou, Y., Roos, C. F. & Zoller, P. Open-system quantum simulation with trapped ions. *In preparation* (2010)

[45] Nayak, C., Simon, S. H., Stern, A., Freedman, M. & Das Sarma, S. Non-abelian anyons and topological quantum computation. *Rev. Mod. Phys.* **80**, 1083–1159 (2008)

[46] Moessner, R. & Sondhi, S. L. Resonating valence bond phase in the triangular lattice quantum dimer model. *Phys. Rev. Lett.* **86**, 1881–1884 (2001)

[47] Ralph, T. C., Bartlett, S. D., OBrien, J. L., Pryde, G. J. & Wiseman, H. M. Quantum nondemolition measurements for quantum information. *Phys. Rev. A* **73**, 012113 (2006)

[48] Fleming, G. R., Huelga, S. & Plenio, M., editors. *Focus on Quantum Effects and Noise in Biomolecules, New J. Phys.*, volume 12. Institute of Physics (2010)

[49] R. Schmied, J. H. W. & Leibfried, D. Optimal surface-electrode trap lattices for quantum simulation with trapped ions. *Phys. Rev. Lett.* **102**, 233002 (2009)

[50] Weimer, H., Müller, M., Lesanovsky, I., Zoller, P. & Büchler, H. P. A Rydberg quantum simulator. *Nature Phys.* **6**, 382–388 (2010)

An Open-System Quantum Simulator with Trapped Ions SUPPLEMENTARY INFORMATION

Julio T. Barreiro*[,1], Markus Müller*[,2,3], Philipp Schindler[1], Daniel Nigg[1], Thomas Monz[1], Michael Chwalla[1,2], Markus Hennrich[1], Christian Roos[1,2], Peter Zoller[2,3] and Rainer Blatt[1,2]

[1]Institut für Experimentalphysik, Universität Innsbruck, Technikerstrasse 25, 6020 Innsbruck, Austria
[2]Institut für Quantenoptik und Quanteninformation, Österreichische Akademie der Wissenschaften, Technikerstrasse 21A, 6020 Innsbruck, Austria
[3]Institut für Theoretische Physik, Universität Innsbruck, Technikerstrasse 25, 6020 Innsbruck, Austria
* These authors contributed equally to this work.

CONTENTS

List of tables

I. BELL-STATE COOLING

A. Implemented Kraus maps

The Bell state $|\Psi^-\rangle$ is not only uniquely determined as the simultaneous eigenstate with eigenvalue -1 of the two stabilizer operators X_1X_2 and Z_1Z_2 (as mentioned in the text), but also by X_1X_2 and Y_1Y_2. In the experiment, we implemented cooling into $|\Psi^-\rangle$ by engineering the two Kraus maps $\rho_S \mapsto E_1\rho_S E_1^\dagger + E_2\rho_S E_2^\dagger$ and $\rho_S \mapsto E_1'\rho_S {E_1'}^\dagger + E_2'\rho_S {E_2'}^\dagger$, where

$$E_1 = \sqrt{p}\, Y_1 \frac{1}{2}\left(1 + X_1X_2\right),$$
$$E_2 = \frac{1}{2}\left(1 - X_1X_2\right) + \sqrt{1-p}\,\frac{1}{2}\left(1 + X_1X_2\right),$$
$$E_1' = \sqrt{p}\, X_1 \frac{1}{2}\left(1 + Y_1Y_2\right),$$
$$E_2' = \frac{1}{2}\left(1 - Y_1Y_2\right) + \sqrt{1-p}\,\frac{1}{2}\left(1 + Y_1Y_2\right),$$

which generate pumping into the -1 eigenspaces of X_1X_2 and Y_1Y_2 (instead of pumping into the eigenspaces of X_1X_2 and Z_1Z_2 as explained in Box 1 of the main text). The reason for pumping into the eigenspaces of X_1X_2 and Y_1Y_2 is that the mapping and unmapping steps, shown as (i) and (iii) in Box 1, are realized by a single MS gate $U_{X^2}(\pi/2)$ and $U_{Y^2}(\pi/2)$, respectively.

B. Circuit decomposition

The map for pumping into the -1 eigenspace of X_1X_2 was implemented by the unitary

$$U_{X^2(\pi/2)}\, C(p)\, U_{X^2(\pi/2)} \tag{1}$$

(corresponding to steps (i) - (iii) in Box 1) followed by an optical pumping of the ancilla qubit to $|1\rangle$. Here, the two-qubit controlled gate is

$$\begin{aligned} C(p) &= |0\rangle\langle 0|_0 \otimes \exp(i\alpha Z_1) + |1\rangle\langle 1|_0 \otimes \mathbb{1} \\ &= \exp\left[\frac{1}{2}(1+Z_0)i\alpha Z_1\right] \\ &= U_{Z_1}(-\alpha)\, U_Y(\pi/2)\, U_{X^2}^{(0,1)}(-\alpha)\, U_Y(-\pi/2) \end{aligned} \tag{2}$$

where $U_{X^2}^{(0,1)}(-\alpha) = \exp(i(\alpha/2)X_0X_1)$ denotes an MS gate acting only on the ancilla and the first system qubit. This two-qubit MS gate operation was implemented in the experiment by the use of refocusing techniques (Nebendahl *et al.*, 2009). In more detail, the gate $U_{X^2}^{(0,1)}$ was realized by interspersing two of the available three-qubit MS gate operations with single-ion light

shifts on the second system qubit which induces a π-phase shift between the qubit states. Alternatively, this refocusing could be avoided, and the sequences further simplified, by hiding the population of individual ions (here the second system ion) which are not supposed to participate in collective coherent operations in electronic levels decoupled from the driving laser excitation. More details on how to systematically decompose Kraus maps into the experimentally available ion-trap gate operations, in particular the multi-ion MS entangling gate, can be found in (Müller *et al.*, 2010).

The circuit decompositions for the experimental implementation of the two maps are shown in Fig. S1. We note that the circuits have been simplified at the expense of implementing in addition in each dissipative map a flip operation Y_1Y_2 on the two system qubits. However, as this additional unitary corresponds to one of the stabilizers into whose -1 eigenspace cooling is performed, this does not interfere with the cooling dynamics.

Cooling with unit pumping probability $p = 1$ corresponds to $\alpha = \pi/2$, whereas $p = 0.5$ is realized with by setting $\alpha = \pi/4$. In the experiment, the "fundamental" MS gate was calibrated to implement $U_{X^2}(\alpha/2)$. The fully entangling operation $U_{X^2}(\pi/2)$ at the beginning and the end of the sequence Fig. S1a was then implemented by applying the $U_{X^2}(\alpha/2)$ operation twice (for $p = 1$) or four times (for $p = 0.5$). The fully entangling operations $U_{Y^2}(\pi/2)$ in Fig. S1b were implemented by two- and four-fold application of the "fundamental" MS gate with a shifted optical phase of the driving laser (cf. Section 2 in the main text).

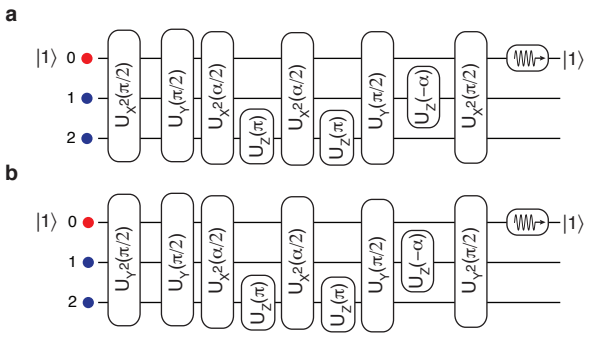

FIG. S1 **Experimental sequences for Bell-state cooling.** Pumping into the eigenspaces of eigenvalue -1 of X_1X_2 (circuit **a,**) and Y_1Y_2 (circuit **b,**) occurs with a probability p in each step, where $\sin^2\alpha = p$.

C. Additional data

The initially mixed state was prepared with a fidelity of F=99.6(3)% with respect to the ideal state $\frac{1}{4}\mathbb{1}_{4\times4}$.

Physical process matrices were reconstructed with maximum likelihood techniques (Jezek *et al.*, 2003). An error analysis was carried out via Monte Carlo simulations over the multinomially distributed measurement outcomes of the state and process tomography. For each process and state, 200 Monte Carlo samples were generated and reconstructed via maximum-likelihood estimation.

II. FOUR-QUBIT STABILIZER PUMPING

Expectation values of the stabilizer operators Z_1Z_2, Z_2Z_3, Z_3Z_4 and $X_1X_2X_3X_4$ were not determined from the reconstructed density matrices of the system qubits. Instead, we performed fluorescence measurements in the X and Z basis on 5250 copies of the corresponding quantum states (for $p = 0.5$ cooling, 2100 copies were measured). The error bars were then determined from the multinomially distributed raw data.

A. Cooling

Cooling into the GHZ state $(|0000\rangle + |1111\rangle)/\sqrt{2}$ was realized by a pumping cycle where the four system qubits were deterministically pumped into the +1 eigenspaces of the stabilizers Z_1Z_2, Z_2Z_3, Z_3Z_4 and $X_1X_2X_3X_4$.

Pumping into the -1 eigenspace of Z_1Z_2 in the first cooling step could be achieved in complete analogy with Bell state cooling, i.e. by implementing a dissipative map, which only involves operations on the ancilla qubit and the system qubits #1 and #2, whereas the system qubits #3 and #4 remain completely unaffected. This could either be achieved through refocusing techniques or by hiding system ions #3 and #4 in electronically decoupled states for the duration of the dissipative circuit.

In the experiment, however, we used a few simplications, which are schematically shown in Fig. S2 and listed below:

- For deterministic cooling ($p = 1$), the inverse mapping step (shown in Box 1) is not necessary and has been taken out.
- In the coherent mapping step (shown in Box 1) the information about whether the system ions are in a ±1 eigenstate of Z_1Z_2 is mapped onto the logical states of the ancilla qubit. This step ideally only involves the ancilla and the system qubits #1 and #2. One way to achieve this three-qubit operation without affecting the system qubits #3 and #4, is to combine the available five-ion MS gate with appropriately chosen refocusing pulses, i.e. light shift operations on individual ions. Those would have to be chosen such that ions #0, #1 and #2 become decoupled from ions #3 and #4, and furthermore residual interactions between ions #3 and #4 cancel out. However, it turns out that residual inter-

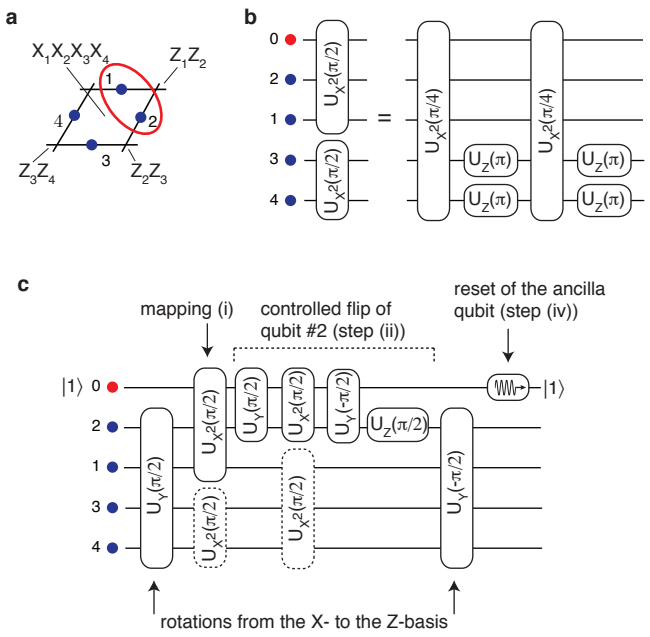

FIG. S2 **Pumping into the +1 eigenspace of the Z_1Z_2 stabilizer operator a,** Ideally, only the ancilla qubit and the two system qubits #1 and #2 are involved in the circuit. **b,** An entangling gate acting on these three ions can be achieved by a refocusing technique, where ions #3 and #4 decouple from the dynamics. However, the latter ions still become entangled. However, these residual interactions are not harmful to the cooling, as they do not affect the expectation values of the other two-qubit stabilizer operators. **c,** Dashed operations in the quantum circuit indicate such residual entangling operations.

actions between ions #3 and #4 can be tolerated: although not required for the Z_1Z_2-pumping dynamics, they are not harmful, as they do not alter the expectation values of the other two-qubit stabilizers Z_2Z_3 and Z_3Z_4. In our experiment the decoupling of ions #0, #1 and #2 from the ions #3 and #4 was achieved by the circuit shown in Fig. S2b.

The additional interactions in the pumping of the two-qubit stabilizer operators Z_iZ_j affect the state of the system qubits with respect to the four-qubit stabilizer $X_1X_2X_3X_4$. However, this effect is not detrimental to the cooling, provided the pumping into the eigenspace of $X_1X_2X_3X_4$ is performed as the final step in the cooling cycle.

- In the employed sequence, the number of single-qubit rotations was reduced wherever possible. Essential single-qubit light shift operations, such as those needed for re-focusing operations, were kept.

- Local rotations of the system ions at the end of a cooling step, which would be compensated at the beginning of the subsequent cooling step, were omitted when several dissipative maps were applied in a row. The corresponding gates of the sequences are displayed in blue in Steps 1-3.

These simplifications allowed us to significantly reduce the length and complexity of the employed gate sequences for one stabilizer pumping step. The compressed gate sequences as used in the experiment are explicitly given below.

Step 1 (pumping into the +1 eigenspace of Z_1Z_2):

$$\begin{aligned}
&U_Y(-\pi/2)\,U_{Z_2}(-\pi/2)\\
&U_X(\pi/2)\,U_{Z_2}(-\pi/2)\,U_X(-\pi/2)\\
&U_{Z_1}(\pi)\,U_{X^2}(\pi/4)\,U_{Z_2}(\pi)\,U_{Z_0}(\pi)\,U_{X^2}(\pi/4)\\
&U_X(-\pi/2)\,U_{Z_2}(-\pi/2)\,U_{Z_0}(-\pi/2)\,U_X(\pi/2)\\
&U_{X^2}(\pi/4)\,U_{Z_4}(\pi)\,U_{Z_3}(\pi)\,U_{X^2}(\pi/4)\\
&U_Y(\pi/2)\,U_X(-\pi/2)\,U_{Z_0}(-\pi/2)\,U_X(\pi/2)
\end{aligned}$$

Step 2 (pumping into the +1 eigenspace of Z_2Z_3):

$$\begin{aligned}
&U_Y(-\pi/2)\,U_{Z_3}(-\pi/2)\\
&U_X(\pi/2)\,U_{Z_3}(-\pi/2)\,U_X(-\pi/2)\\
&U_{Z_2}(\pi)\,U_{X^2}(\pi/4)\,U_{Z_3}(\pi)\,U_{Z_0}(\pi)\,U_{X^2}(\pi/4)\\
&U_X(-\pi/2)\,U_{Z_3}(-\pi/2)\,U_{Z_0}(-\pi/2)\,U_X(\pi/2)\\
&U_{X^2}(\pi/4)\,U_{Z_4}(\pi)\,U_{Z_1}(\pi)\,U_{X^2}(\pi/4)\\
&U_Y(\pi/2)\,U_X(-\pi/2)\,U_{Z_0}(-\pi/2)\,U_X(\pi/2)
\end{aligned}$$

Step 3 (pumping into the +1 eigenspace of Z_3Z_4):

$$\begin{aligned}
&U_Y(-\pi/2)\,U_{Z_4}(-\pi/2)\\
&U_X(\pi/2)\,U_{Z_4}(-\pi/2)\,U_X(-\pi/2)\\
&U_{Z_3}(\pi)\,U_{X^2}(\pi/4)\,U_{Z_4}(\pi)\,U_{Z_0}(\pi)\,U_{X^2}(\pi/4)\\
&U_X(-\pi/2)\,U_{Z_4}(-\pi/2)\,U_{Z_0}(-\pi/2)\,U_X(\pi/2)\\
&U_{X^2}(\pi/4)\,U_{Z_2}(\pi)\,U_{Z_1}(\pi)\,U_{X^2}(\pi/4)\\
&U_Y(\pi/2)\,U_X(-\pi/2)\,U_{Z_0}(-\pi/2)\,U_X(\pi/2)
\end{aligned}$$

Step 4 (pumping into the +1 eigenspace of $X_1X_2X_3X_4$):

$$\begin{aligned}
&U_X(-\pi/2)\\
&U_{Z_4}(-\pi/2)\,U_X(\pi/2)\,U_{Z_4}(-\pi/2)\\
&U_{X^2}(\pi/4)\,U_{Z_4}(\pi)\,U_{Z_0}(\pi)\,U_{X^2}(\pi/4)\\
&U_{Z_4}(-\pi/2)\,U_X(-\pi/2)\,U_{Z_0}(-\pi/2)\,U_X(\pi/2)\\
&U_{X^2}(\pi/4)\,U_{X^2}(\pi/4)
\end{aligned}$$

Figure S10 shows the reconstructed density matrices (real and imaginary parts) for every step of the cooling cycle. The complete circuit decomposition of one cooling cycle involves 16 five-ion entangling operations, 28 (20) collective unitaries and 36 (34) single-qubit operations with (without) optional operations in blue. The reset operation involves further pulses not accounted for above.

B. Repeated four-qubit stabilizer pumping

To study the robustness of the dissipative operation, we prepared the initial state $|1111\rangle$ and subsequently applied repeatedly the dissipative map for pumping into the $+1$ eigenspace of the four-qubit stabilizer $X_1X_2X_3X_4$. We observed that after a single dissipative step a non-zero expectation value of $X_1X_2X_3X_4$ built up and stayed constant under subsequent applications of this dissipative map. However, due to imperfections in the gate operations, the expectation values of the two-qubit stabilizers decreased, ideally they should not be affected by the $X_1X_2X_3X_4$-pumping step (see Fig. S3). Interestingly, the expectation values of Z_1Z_4 and Z_3Z_4 decayed significantly faster than those for Z_1Z_2 and Z_2Z_3. This decay can be explained by the fact that in the gate sequence used for pumping into the $+1$ eigenspace of $X_1X_2X_3X_4$, step 4 above, single-ion light-shift operations are applied only to the fourth system qubit and the ancilla. This indicates that errors in the single-qubit gates applied to the fourth system ion accumulate under the repeated application of the dissipative step, and thus affect the stabilizers Z_1Z_4 and Z_3Z_4 which involve this system qubit more strongly than the others. This destructive effect can be minimized by alternating the roles of the system qubits.

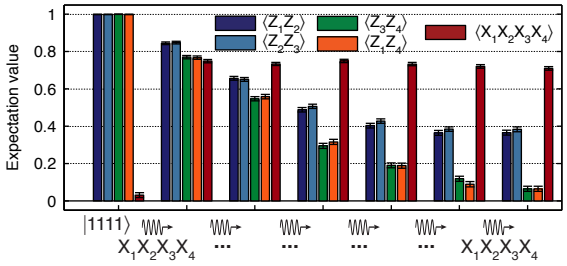

FIG. S3 **Measured expectation value of stabilizers for repeated pumping without sequence optimization.** The expectation values of Z_1Z_4 and Z_3Z_4 show a significantly faster decay than those for Z_1Z_2 and Z_2Z_3. In every step of the cooling, most single-ion light-shift operations are applied to the fourth system qubit.

Such optimization has been done for the dissipative dynamics shown in Fig. S4. Here, starting from the initial state $|1111\rangle$, repeated pumping into the -1 eigenspace of $X_1X_2X_3X_4$ has been implemented by the sequence

$$\begin{aligned}
&U_{X^2}(\pi/8)\,U_{X^2}(\pi/8)\,U_{X^2}(\pi/8)\,U_{X^2}(\pi/8)\\
&U_X(-\pi/2)\\
&U_{Z_4}(-\pi/2\times p)\,U_X(\pi/2)\,U_{Z_4}(\pi)\\
&U_{Y^2}(\pi/4\times p)\,U_{Z_0}(\pi)\,U_{Z_4}(\pi)\,U_{Y^2}(\pi/4\times p)\\
&U_Y(\pi/2)\,U_{Z_0}(-\pi/2)\,U_Y(-\pi/2)\\
&U_{X^2}(\pi/8)\,U_{X^2}(\pi/8)\,U_{X^2}(\pi/8)\,U_{X^2}(\pi/8)
\end{aligned}$$

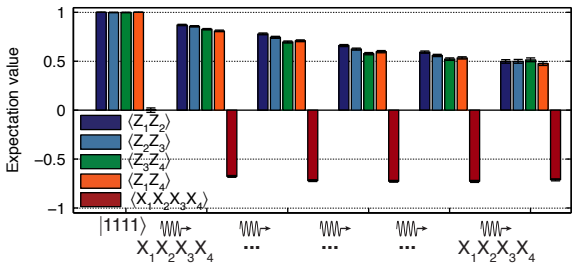

FIG. S4 **Measured expectation value of stabilizers for repeated pumping with sequence optimization.** All two-qubit stabilizers decay at the same rate during cooling. In step 1,2,3,4, and 5 the single-qubit light-shift operations were applied on the system qubits 4,3,2,1, and 1, respectively.

Here, we observed that indeed the expectation values of all two-qubit stabilizers decreased at the same pace and at a slightly slower rate (see Fig. S4). Upon repeating the sequence above 1,2,3,4, and 5 times, we changed the operations shown in red to act on qubits 4,3,2,1, and 1, respectively. The stabilizer expectation values for deterministic cooling, or $p = 1$, are shown in Fig. S4.

C. Pushing "anyons" around

In Kitaev's toric code (Kitaev, 2003), spins are located on the edges of a two-dimensional square lattice. The Hamiltonian

$$H = -g(\sum_p A_p + \sum_v B_p) \tag{3}$$

is a sum of mutually commuting four-qubit stabilizers $A_p = \prod_{i\in p} X_i$ and $B_v = \prod_{i\in v} Z_i$, which describe four-spin interactions between spins located around plaquettes p and vertices v of the lattice. The ground state of the Hamiltonian is the simultaneous $+1$ eigenstate of all stabilizer operators. The model supports two types of excitations that obey anyonic statistics under exchange (braiding), and they correspond to -1 eigenstates of either plaquette or vertex stabilizers.

For a minimal instance of this model, represented by a single plaquette of four spins located on the edges, the Hamiltonian contains a single four-qubit interaction term $X_1X_2X_3X_4$ and pairwise two-spin interactions Z_iZ_j of spins sharing a corner of the plaquette. The ground state as the simultaneous $+1$ eigenstate of these stabilizers is the GHZ-state $(|0000\rangle + |1111\rangle)/\sqrt{2}$. States corresponding to -1 eigenvalues of a two-qubit stabilizer Z_iZ_j can be interpreted as a configuration with an excitation located at the corner between the two spins i and j. Similarly, a four-qubit state with an eigenvalue of -1 with respect to $X_1X_2X_3X_4$, would correspond to an anyonic excitation located at the center of the plaquette.

In the experiment we prepared an initial state $|0111\rangle$ and then performed the cooling cycle of four deterministic pumping steps into the +1 eigenspaces of Z_1Z_2, Z_2Z_3, Z_3Z_4 and $X_1X_2X_3X_4$, using the sequences for Steps 1 to 4 given in section II.A. The expectation values of the stabilizer operators for the initial state and the four spins after each pumping step are shown in Fig. S5. The dissipative dynamics can be visualized as follows: For the initial state with $\langle Z_1Z_2\rangle = -1$ and $\langle Z_1Z_4\rangle = -1$ a pair of excitations is located on the upper left and right corners of the plaquette, whereas $\langle X_1X_2X_3X_4\rangle = 0$ implies an anyon of the other type is present at the center of the plaquette with a probability 50%. In the first cooling step, where the first two spins are pumped into the +1 eigenspace of Z_1Z_2, the anyon at the upper right corner is dissipatively pushed to the lower right corner of the plaquette. In the third step of pumping into the +1 eigenspace of Z_3Z_4, the two excitations located on the upper and lower lefts corners fuse and disappear from the system. In the final step of pumping into the +1 eigenspace of $X_1X_2X_3X_4$, the anyon with a probability of 50% at the center of the plaquette is pushed out from the plaquette.

However, we'd like to stress that borrowing concepts from topological spin models, such as anyonic excitations, here is merely a convenient language to phrase and visualize the dissipative dynamics. In the present work with up to five ions, we do *not* explore the physics of topological spin models, since (i) in a minimal system of four spins the concepts developed for larger lattice models become questionable, and more importantly, (ii) during the implemented cooling dynamics the underlying (four-body) Hamiltonian of the model was not present. We rather demonstrate the basic tools which will allow one to explore this physics once larger, two-dimensional systems become available in the laboratory.

We note that photon experiments have reported the observation of correlations compatible with the manipulations of "anyons" in a setup representing two plaquettes (Lu *et al.*, 2009; Pachos *et al.*, 2009). Such experiments are based on postselection of measurements (as in teleportation by Bouwmeester *et al.*, 1997), which should be contrasted to our deterministic implementation of open system dynamics to prepare and manipulate the corresponding quantum state (as in deterministic teleportation by Barrett *et al.*, 2004; Riebe *et al.*, 2004).

D. Pumping into "excited" states

Starting from an initially fully mixed state of four qubits, we also implemented cooling into a different GHZ-type state, $(|0010\rangle - |1101\rangle)/\sqrt{2}$, by a sequence of four dissipative steps: 1) pumping into the +1 eigenspace of Z_1Z_2, 2) pumping into the -1 eigenspace of Z_2Z_2, 3) pumping into the -1 eigenspace of Z_3Z_4 and 4) pumping into the -1 eigenspace of $X_1X_2X_3X_4$. In the context of Kitaev's toric code, this state would correspond to an excited state. However, as above, we point out that the underlying Hamiltonian was not implemented in the cooling dynamics.

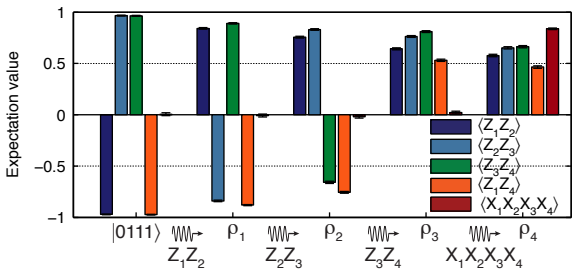

FIG. S5 **Pushing "anyons" around by dissipation.** Measured expectation values of stabilizer operators for cooling dynamics of pumping into the +1 eigenspaces of Z_1Z_2, Z_2Z_3, Z_3Z_4 and $X_1X_2X_3X_4$, starting in the state $|0111\rangle$.

The measured expectation values of the stabilizers are shown in Fig. S6. The final density matrix, as determined from quantum state tomography after the four cooling steps, is shown in Fig. S7. This cooling cycle was implemented with the same sequences as given for Step 1 to 4 in section II.A, with the only difference that the sign of the phase shift operations displayed in red was changed in Steps 2, 3, and 4. This allowed us to invert the pumping direction from the +1 into -1 eigenspaces of Z_2Z_2, Z_3Z_4 and $X_1X_2X_3X_4$.

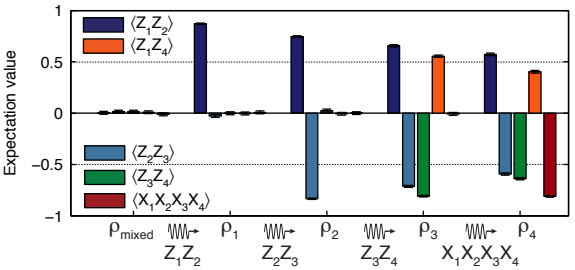

FIG. S6 **Cooling into an "excited" state.** Measured expectation values of two- and four-qubit stabilizer operators for pumping into the state $(|0010\rangle - |1101\rangle)/\sqrt{2}$, starting from an initially four-qubit mixed state.

III. QND MEASUREMENT OF A FOUR-QUBIT STABILIZER

A. Further details

As shown in Fig. S8, the QND measurement involves a mapping step where the information about whether the system described by an input density matrix ρ^{in} is in

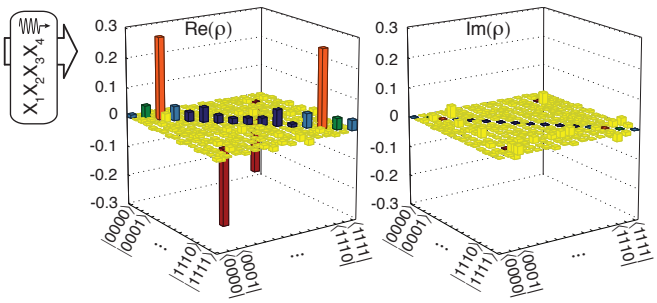

FIG. S7 **Reconstructed density matrix after the full cooling cycle for dissipative preparation of the state** $(|0010\rangle - |1101\rangle)/\sqrt{2}$**.** This final state has a fidelity of 60(2)% with the expected state. This fidelity was determined from parity and coherence measurements and analysed with bayesian inference techniques as done in (Monz *et al.*, 2010).

the +1 / -1 eigenspace of $A = X_1X_2X_3X_4$ is coherently mapped onto the internal states $|0\rangle$ and $|1\rangle$ of the ancilla qubit, which is initially prepared in $|1\rangle$. Subsequently the ancilla qubit is measured in its computational basis, leaving the system qubits in a corresponding output state $\rho^{\rm out}$.

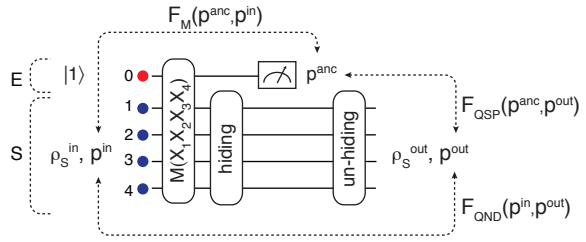

FIG. S8 **QND measurement of the four-qubit stabilizer operator** $X_1X_2X_3X_4$**.** After the coherent mapping $M(X_1X_2X_3X_4)$, the ancilla qubit is measured. This measurement was performed both with and without applying additional pulses to hide the populations of the system qubits in electronically uncoupled states for the duration of the fluorescence measurement on the ancilla.

The coherent mapping $M(X_1X_2X_3X_4)$ was realized by the sequence

$$\begin{aligned} &U_X(\pi/4)U_{Z_0}(\pi)\,U_X(-\pi/4)\\ U_{X^2}(\pi/4)\,U_{X^2}(\pi/4)\,&U_{Z_0}(-\pi/2)\,U_{X^2}(\pi/4)\,U_{X^2}(\pi/4)\\ &U_Y(-\pi/4)\,U_{Z_0}(\pi)\,U_Y(\pi/4) \end{aligned}$$

which implements

$$\begin{aligned} M(X_1X_2X_3X_4) = &-\frac{i}{\sqrt{2}}(X_0+Y_0)\otimes P_+\\ &+\frac{1}{\sqrt{2}}(1-iZ_0)\otimes P_-, \end{aligned} \qquad (4)$$

with $P_\pm = \frac{1}{2}(1\pm X_1X_2X_3X_4)$ the projectors onto the ±1 eigenspaces of $X_1X_2X_3X_4$. Equation (4) shows that for the system qubits being in a state belonging to the +1 eigenspace of the stabilizer operator, the ancilla is flipped from $|1\rangle$ to $|0\rangle$, whereas it remains in its initial state $|1\rangle$ otherwise.

Subsequently, the ancilla as well as the four system qubits were measured. This was done by measuring the five ions simultaneously. Alternatively, we first hid the four system qubits in electronic levels decoupled from the laser excitation, performed the fluorescence measurement of the ancilla qubit, then recovered the state of the system qubits and tomographically measured the state of the four system qubits. The second approach, where the state of the system is not affected by the measurement of the ancilla, is of importance if the information from the ancilla measurement is to be used for feedback operations on the state of the system.

B. Quantitative analysis of the performance

To characterize the performance of a QND measurement for a (multi-)qubit system, a set of requirements and corresponding fidelity measures have been discussed in the literature (Ralph *et al.*, 2006).

(1) First of all, the measurement outcomes for the ancilla qubit should agree with those that one would expect from a direct measurement of the observable A on the input density matrix. This property can be quantified by the *measurement fidelity*,

$$F_{\rm M} = \left(\sqrt{p^{\rm in}_+ p^{\rm m}_{|0\rangle}} + \sqrt{p^{\rm in}_- p^{\rm m}_{|1\rangle}}\right)^2, \qquad (5)$$

which measures the correlations of the distribution of measurement outcomes $p^{\rm m} = \{p^{\rm m}_{|0\rangle}, p^{\rm m}_{|1\rangle}\}$ of the ancilla qubit with the expected distribution $p^{\rm in} = \{p^{\rm in}_+, p^{\rm in}_-\}$ directly obtained from $\rho^{\rm in}$, where $p^{\rm in}_\pm = {\rm Tr}\{\frac{1}{2}(1\pm A)\rho^{\rm in}\}$.

(2) The QND character, reflected by the fact that the observable A to be measured should not be disturbed by the measurement itself, becomes manifest in ideally identical probability distributions $p^{\rm in}$ and $p^{\rm out}$, which are determined from the input and output density matrices. These correlations are quantified by the *QND fidelity*

$$F_{\rm QND} = \left(\sqrt{p^{\rm in}_+ p^{\rm out}_+} + \sqrt{p^{\rm in}_- p^{\rm out}_-}\right)^2, \qquad (6)$$

where $p^{\rm out}_\pm = {\rm Tr}\{\frac{1}{2}(1\pm A)\rho^{\rm out}\}$.

(3) Finally, by measuring the ancilla qubit the system qubits should be projected onto the corresponding eigenspace of the measured observable A. Thus the quality of the QND measurement as a quantum state preparation (QSP) device is determined by the correlations between the ancilla measurement outcomes and the corresponding system output density matrices. It can be described by the *QSP fidelity*

$$F_{\rm QSP} = p^{\rm m}_+ p^{\rm out}_{|0\rangle,+} + p^{\rm m}_- p^{\rm out}_{|1\rangle,-}, \qquad (7)$$

where $p^{\mathrm{out}}_{|0/1\rangle,\pm}$ denotes the conditional probability of finding the system qubits in the +1 (-1) eigenspace of A, provided the ancilla qubit has been previously measured in $|0\rangle$ ($|1\rangle$).

The probability distributions for the system input and output states, the ancilla measurement outcome distributions, and the resulting fidelity values are summarized in Tables I to IV. The input states had a fidelity (Jozsa, 1994) with the ideal states $(|0000\rangle + |1111\rangle)/\sqrt{2}$, $(|0000\rangle - |1111\rangle)/\sqrt{2}$ and $(|0011\rangle - |1100\rangle)/\sqrt{2}$ of $75.3(9), 77.3(8), 93.2(4)\%$.

We observe that we obtain higher values for the measurement and QND fidelities than for the QSP fidelities. The latter is relevant in the context of quantum error correction or closed-loop simulation protocols or more generally whenever the information from the ancilla measurement is used for further processing of the system output state.

With the additional hiding and unhiding pulses before and after the measurement of the ancilla we observe a loss of fidelity of a few percent in the QSP fidelities.

TABLE I QND probability distributions. Obtained from measurements **with** hiding of the system ions during the measurement of the ancilla.

input state	eigenspace	p^m_{in}	p^m_{out}	p^{in}	$p^{in}_{m=0}$	$p^{in}_{m=1}$	p^{out}	$p^{out}_{m=0}$	$p^{out}_{m=1}$
$\|0000\rangle + \|1111\rangle$	$+1$	0.959(1)	0.847(3)	0.817(9)	0.822(9)	0.618(34)	0.689(12)	0.736(12)	0.359(34)
	-1	0.041(1)	0.153(3)	0.183(9)	0.178(9)	0.382(34)	0.311(12)	0.264(12)	0.641(34)
$\|0000\rangle - \|1111\rangle$	$+1$	0.955(1)	0.169(3)	0.191(10)	0.187(9)	0.328(36)	0.310(11)	0.640(26)	0.242(12)
	-1	0.045(1)	0.831(3)	0.809(10)	0.813(9)	0.672(36)	0.690(11)	0.360(26)	0.758(12)
$\|0011\rangle - \|1100\rangle$	$+1$	0.978(1)	0.103(2)	0.041(4)	0.035(4)	0.412(47)	0.137(9)	0.476(36)	0.097(7)
	-1	0.022(1)	0.897(2)	0.959(4)	0.965(4)	0.588(47)	0.863(9)	0.524(36)	0.903(7)

TABLE II QND probability distributions. Obtained from measurements **without** hiding of the system ions during the measurement of the ancilla.

input state	eigenspace	p^m_{out}	p^{out}	$p^{out}_{m=0}$	$p^{out}_{m=1}$
$\|0000\rangle + \|1111\rangle$	$+1$	0.850(3)	0.713(11)	0.789(11)	0.336(30)
	-1	0.150(3)	0.287(11)	0.211(11)	0.664(30)
$\|0000\rangle - \|1111\rangle$	$+1$	0.188(3)	0.265(12)	0.504(28)	0.220(11)
	-1	0.812(3)	0.735(12)	0.496(28)	0.780(11)
$\|0011\rangle - \|1100\rangle$	$+1$	0.099(2)	0.073(7)	0.416(35)	0.038(5)
	-1	0.901(2)	0.927(7)	0.584(35)	0.962(5)

TABLE III QND figures of merit. Determined from measurements **with** hiding of the system ions during the measurement of the ancilla. Since the state $|0011\rangle - |1100\rangle$ is particularly robust against decoherence, the fidelity $F_{\rm QSP}$ is higher, as shown for 8 ions in (Monz *et al.*, 2010).

input state	eigenspace	$p^{\rm in}$	$p^{\rm out}$	$p^{\rm m}$	$p^{\rm out}_{\rm QND=+}$	$p^{\rm out}_{\rm QND=-}$	$F_{\rm M}(p^{\rm in},p^{\rm m})$	$F_{\rm QND}(p^{\rm in},p^{\rm out})$	$F_{\rm QSP}(p^{\rm m},p^{\rm out}_{\rm QND})$
$\|0000\rangle + \|1111\rangle$	$+1$	0.82(1)	0.69(1)	0.85	0.74(1)		0.998(1)	0.978(5)	0.72(1)
	-1	0.18(1)	0.31(1)	0.15		0.64(3)			
$\|0000\rangle - \|1111\rangle$	$+1$	0.19(1)	0.31(1)	0.17	0.64(3)		0.999(1)	0.980(5)	0.74(1)
	-1	0.81(1)	0.69(1)	0.83		0.76(1)			
$\|0011\rangle - \|1100\rangle$	$+1$	0.041(4)	0.14(1)	0.10	0.48(4)		0.985(3)	0.969(6)	0.86(1)
	-1	0.959(4)	0.86(1)	0.90		0.90(1)			
$\|1111\rangle$	$+1$	0.5	0.47(1)	0.50049	0.70(1)		1	0.9992(6)	0.73(1)
	-1	0.5	0.53(1)	0.49951		0.76(1)			

REFERENCES

Barrett, M. D., J. Chiaverini, T. Schaetz, J. Britton, W. M. Itano, J. D. Jost, E. Knill, C. Langer, D. Leibfried, R. Ozeri, and D. J. Wineland, 2004, Nature **429** (6993), 737.

Bouwmeester, D., *et al.*, 1997, Nature **390**, 575.

Gilchrist, A., N. K. Langford, and M. A. Nielsen, 2005, Phys. Rev. A **71**, 062310.

Jezek, M., J. Fiurasek, and Z. Hradil, 2003, Phys. Rev. A **68** (1), 012305.

Jozsa, R., 1994, J. Mod. Opt. **41** (12), 2315.

Kitaev, A. Y., 2003, Ann. Phys. **303** (1), 2.

Lu, C.-Y., W.-B. Gao, O. Gühne, X.-Q. Zhou, Z.-B. Chen, and J.-W. Pan, 2009, Phys. Rev. Lett. **102** (3), 030502.

Monz, T., *et al.*, 2010, arXiv:1009.6126.

Müller, M., K. Hammerer, Y. Zhou, C. F. Roos, and P. Zoller, 2010, In preparation.

Nebendahl, V., H. Häffner, and C. F. Roos, 2009, Phys. Rev. A **79** (1), 012312.

Pachos, J. K., W. Wieczorek, C. Schmid, N. Kiesel, R. Pohlner, and H. Weinfurter, 2009, New J. Phys. **11** (8), 083010.

Ralph, T. C., S. D. Bartlett, J. L. OBrien, G. J. Pryde, and H. M. Wiseman, 2006, Phys. Rev. A **73** (1), 012113.

Riebe, M., H. Häffner, C. F. Roos, W. Hänsel, J. Benhelm, G. P. T. Lancaster, T. W. Körber, C. Becher, F. Schmidt-Kaler, D. F. V. James, and R. Blatt, 2004, Nature **429** (6993), 734.

TABLE IV QND figures of merit. Determined from measurements **without** hiding of the system ions during the measurement of the ancilla. Since the state $|0011\rangle - |1100\rangle$ is particularly robust against decoherence, the fidelity F_{QSP} is higher, as shown for 8 ions in (Monz *et al.*, 2010).

input state	eigenspace	p^{out}	p^{m}	$p^{\mathrm{out}}_{\mathrm{QND}=+}$	$p^{\mathrm{out}}_{\mathrm{QND}=-}$	$F_{\mathrm{M}}(p^{\mathrm{in}}, p^{\mathrm{m}})$	$F_{\mathrm{QND}}(p^{\mathrm{in}}, p^{\mathrm{out}})$	$F_{\mathrm{QSP}}(p^{\mathrm{m}}, p^{\mathrm{out}}_{\mathrm{QND}})$
$\|0000\rangle + \|1111\rangle$	$+1$	0.71(1)	0.85	0.79(1)		0.998(1)	0.984(4)	0.77(1)
	-1	0.29(1)	0.15		0.66(3)			
$\|0000\rangle - \|1111\rangle$	$+1$	0.26(1)	0.19	0.50(3)		1.0000(1)	0.992(3)	0.73(1)
	-1	0.74(1)	0.81		0.78(1)			
$\|0011\rangle - \|1100\rangle$	$+1$	0.07(1)	0.10	0.42(3)		0.986(2)	0.996(2)	0.91(1)
	-1	0.93(1)	0.90		0.96(1)			
$\|1111\rangle$	$+1$	0.52(1)	0.5078	0.75(1)		0.99994	0.9996(5)	0.74(1)
	-1	0.48(1)	0.4922		0.73(1)			

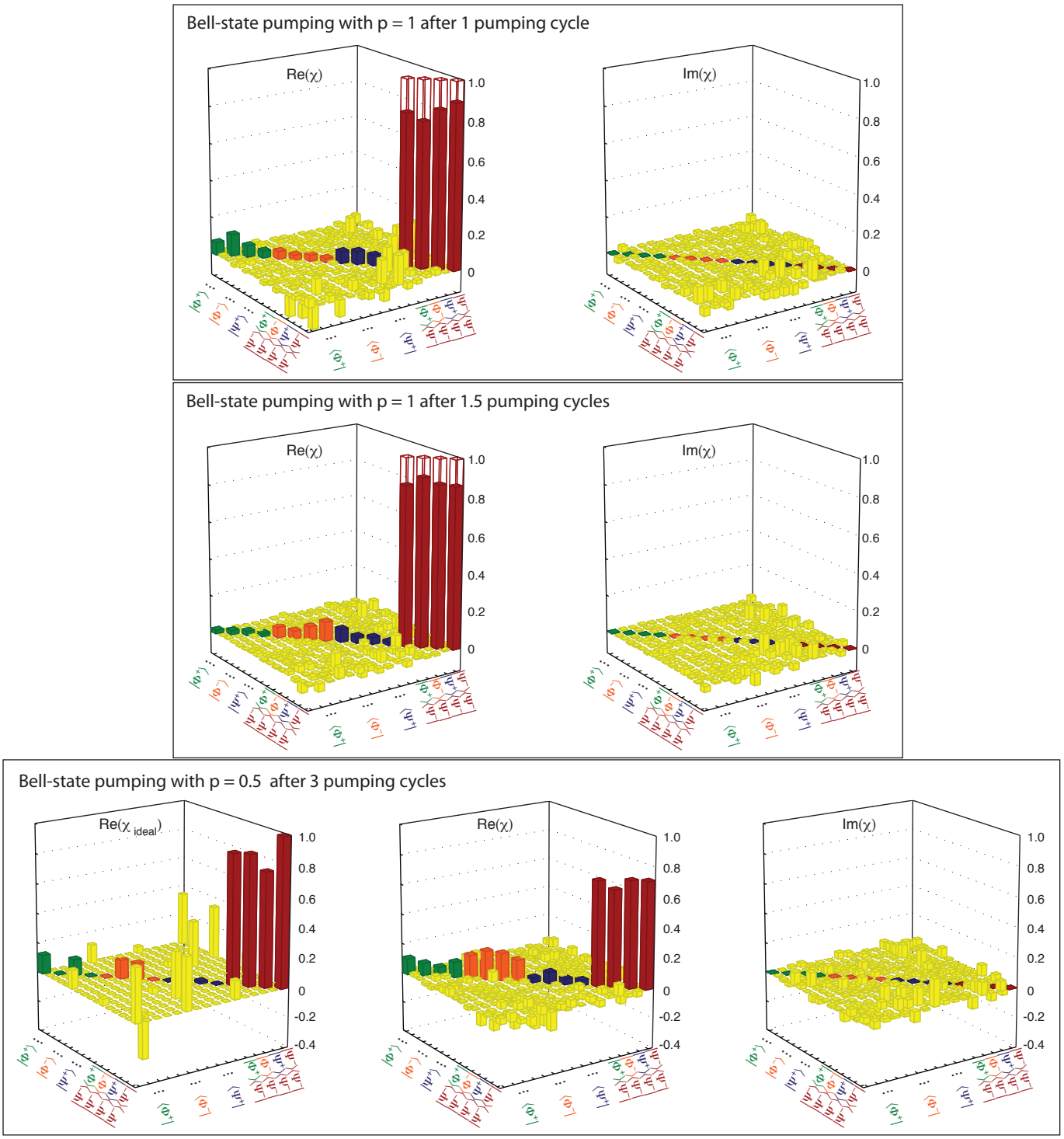

FIG. S9 **Reconstructed process matrices of experimental Bell-state cooling.** The reconstructed process matrix for $p = 1$ after 1 (1.5) cycles has a Jamiolkowski process fidelity (Gilchrist *et al.*, 2005) of 83.4(7)% (87.0(7)%) with the ideal dissipative process $\rho_S \mapsto |\Psi^-\rangle\langle\Psi^-|$ which maps an arbitrary state of the system into the Bell state $|\Psi^-\rangle$. This ideal process has as non-zero elements only the four transparent bars shown. The reconstructed process matrix for $p = 0.5$ after 3 cycles has a Jamiolkowski process fidelity of 60(1)% with the ideal process χ_{ideal} shown [$\text{Im}(\chi_{\text{ideal}}) = 0$].

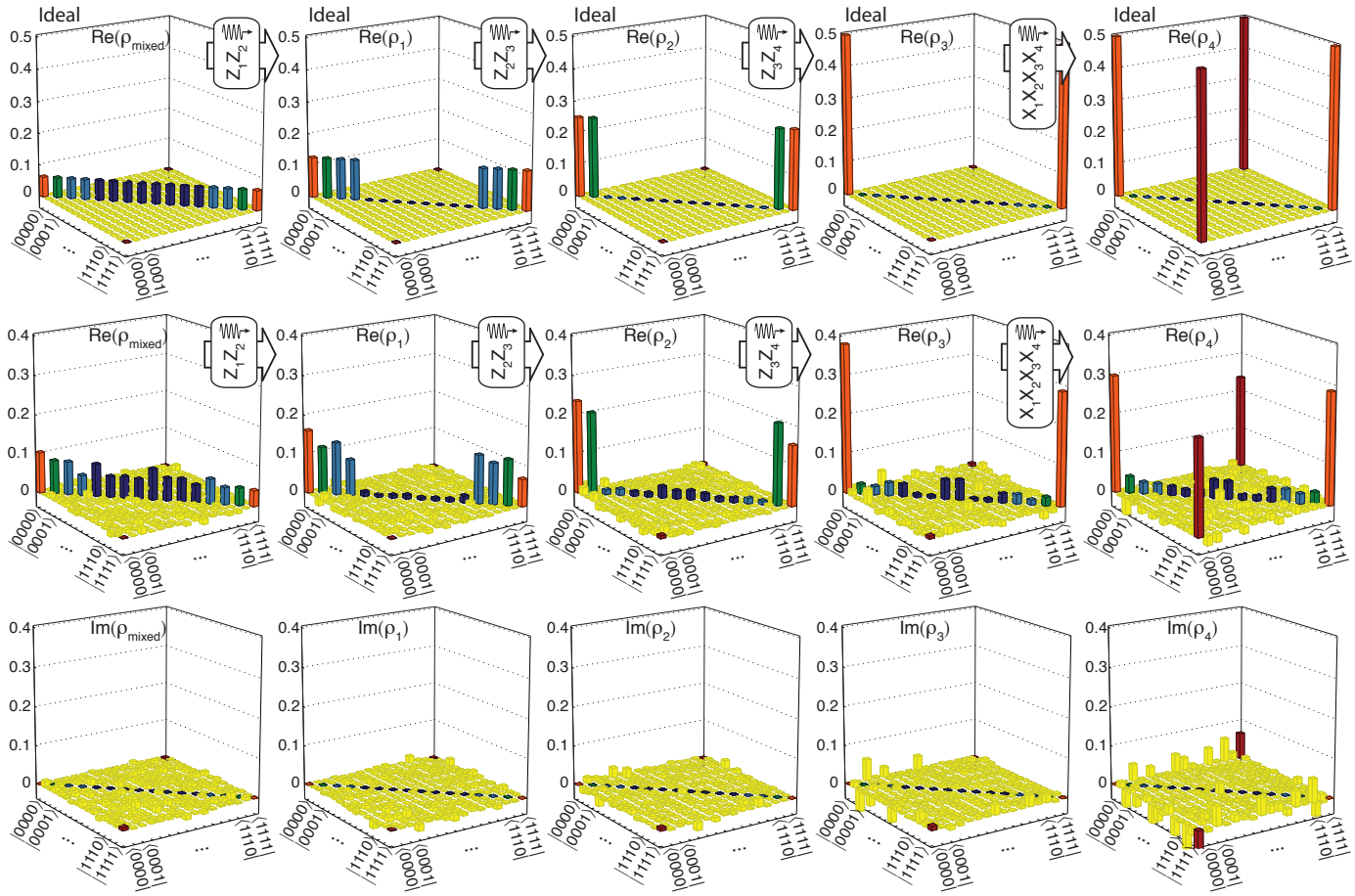

FIG. S10 **Ideal and reconstructed density matrices of plaquette cooling.** An inital mixed state ρ_{mixed} is sequentially pumped by the stabilizers Z_1Z_2, Z_2Z_3, Z_3Z_4 and $X_1X_2X_3X_4$ driving the system into the states $\rho_{1,2,3,4}$.

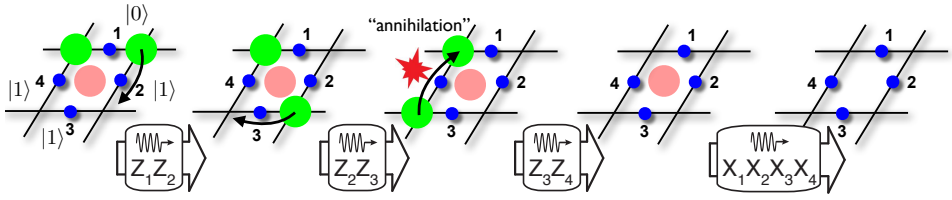

FIG. S11 **Pushing "anyons".** Cartoon of the dissipative dynamics. The pumping dynamics can be visualized by dissipative pushing of excitations (green and red dots) between adjacent corners of the plaquette.